

Molecular HDD Logic for Encrypted Massive Data Storage

Bingjie Guo^{1†}, Xinhui Chen^{1,2†}, An Chen^{1†}, Jinxin Wang^{3†}, Wuhong Xue^{4†}, Tao Wang⁴, Zhixin Wu¹, Xiaolong Zhong¹, Jianmin Zeng¹, Jinjin Li^{1*}, Mao Li^{3,6*}, Xiaohong Xu^{4*}, Yu Chen^{5*}, Gang Liu^{1*}

¹National Key Laboratory of Advanced Micro and Nano Manufacturing Technology, Department of Micro/Nano Electronics, School of Electronic Information and Electrical Engineering, Shanghai Jiao Tong University, Shanghai 200240, China.

²Colleague of Information Engineering, Jinhua University of Vocational Technology, Jinhua 321017, China.

³State Key Laboratory of Polymer Physics and Chemistry, Changchun Institute of Applied Chemistry, Chinese Academy of Sciences, Changchun 130022, China.

⁴Key Laboratory of Magnetic Molecules and Magnetic Information Materials of Ministry of Education, School of Chemistry and Materials Science, Shanxi Normal University, Taiyuan 030031, China

⁵Key Laboratory for Advanced Materials and Joint International Research Laboratory of Precision Chemistry and Molecular Engineering, Feringa Nobel Prize Scientist Joint Research Center, School of Chemistry and Molecular Engineering, East China University of Science and Technology, Shanghai 200273, China

⁶State Key Laboratory of Supramolecular Structure and Materials, College of Chemistry, Jilin University, Changchun 130012, China.

All correspondence should be addressed to: lijinjin@sjtu.edu.cn, limao@jlu.edu.cn, [3148704620@qq.com](tel:3148704620), xuxh@sxnu.edu.cn & gang.liu@sjtu.edu.cn.

ABSTRACT

Organic memories, with small dimension, fast speed and long retention features, are considered as promising candidates for massive data archiving. In order to satisfy the requirements for ultra-low power and high-security information storage, we design a conceptual molecular hard-disk (HDD) logic scheme that is capable to execute *in-situ* encryption of massive data in pW/bit power-consumption range. Beneficial from the coupled mechanism of counter-balanced redox reaction and local ion drifting, the basic HDD unit consisting of ~ 200 self-assembled Ru^XLPH molecules in a monolayer (SAM) configuration undergoes unique conductance modulation with continuous, symmetric and low-power switching characteristics. 96-state memory performance, which allows 6-bit data storage and single-unit one-step XOR operation, is realized in the Ru^XLPH SAM sample. Through single-unit XOR manipulation of the pixel information, *in-situ* bitwise encryption of the Mogao Grottoes mural images stored in the molecular HDD is demonstrated.

INTRODUCTION

The cold storage of massive confidential information in data center coinstantaneously demands high memory density to lower bit cost and high security for anti-hacking purpose. However, the basic units of the traditional hard-disks (HDDs), which are widely used for data archiving, are only capable of encoding binary logic states *via* up- and downward magnetization of the storage media. Operating in a single-bit per cell manner, the data density of such system is severely limited and constrained by the bit size of the magnetic disks. The lack of an effective approach for bit-level encryption of the classified data, on the other hand, deteriorates the security performance of the HDD based storage systems. Organic memories, featured by their small dimension, fast speed and long retention characteristics, are considered as promising candidates of storage-class memory (SCM) for massive data archiving¹⁻⁴. In particular, the versatile conductance states achieved in organic memories not only increase the unit and overall data density of the system, but enable material implemented logic manipulation for high-order information grinding in potential security-concerned applications⁵⁻⁷.

Since the birth in 2003, gigantic efforts have been devoted to developing various physicochemical mechanisms, including electrochemical redox reaction⁸, donor-acceptor charge transfer⁹, nanoparticle-based charge trapping¹⁰, ion migration¹¹, filamentary conduction¹², and conformation reconfiguration¹³, to customize the electronic structures and carrier transport dynamics of organic memory materials. Depending on their diverse conductance switching characteristics, both volatile DRAM, SRAM, and nonvolatile Flash and WORM memory behaviors have been demonstrated in organic devices¹⁴⁻¹⁷. Upon the inclusion

of additional metal complexes or multiple redox active chromophores^{7,18}, coupling between electrochemistry and conformation reconfiguration¹⁹, as well as energy-dependent trapping/detrapping of charge carriers²⁰, consecutive switching behaviors were achieved in organic memory to increase the unit storage density through multi-bit operation. Governing by the solid-state electronic processes occurred in the organic switching layers, modulation of device conductances also endows the possibility of implementing both linear (e.g., AND, OR, NOT) and nonlinear (e.g., NAND and XOR) logic algorithms for bit-by-bit encryption of the stored information^{6,21-25}. Through co-optimizing the compositions, crystalline structures, synthesis approaches and fabrication procedures of organic materials that are compatible with the state-of-the-art CMOS platform over the past decades²⁶⁻³², memory devices with cell dimension down to 2 μm and integrated scale reaching 1024 have been realized to prove their theoretical concept for high density storage applications. Nevertheless, these explorations require to switch a bundle of molecules between different material states to exhibit obvious yet distinguishable device resistances. As a compositive result of the organic assemblies, the high device current in the μA to mA range is extremely undesired for data archiving. Developing organic SCM systems with ultralow power characteristics, as well as being capable of executing more expressive logic functors beyond the conventional Boolean operations, will surely intensify their application toward cold storage of massive confidential information in data center.

As a special example of organic digital gadgets, molecular electronics distinguish themselves with extreme potential for ultrahigh density information storage and logic

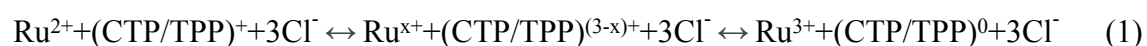
applications³³. Using a single molecule or a few molecules as constituting components to design and construct functional devices on molecular scale, molecular electronics offer a complementary pathway to tussle the ever-coming Moore's predicament³⁴⁻⁴⁰. Peculiarly, manipulating electronic characteristics of a trifle of organic molecules may only consume tiny energy, ideally solving the high-power straits of the organic memories⁴¹. In this contribution, we report the first molecular hard-disk logic scheme that is based on self-assembly monolayer (SAM) of an organometallic complex molecule (OCM). Adopting the conductive-atomic force microscopic (C-AFM) tip with frontend radius of 25 nm as a programming head to write and read the material state encoded digital information, each basic storage unit contains only ~ 200 OCMs of Ru^XLPH. Benefiting from the incorporation of redox-active transitional metal cation (Ru^{x+}), organic ligands of carbazolyl terpyridine (CTP) and terpyridyl phosphonate (TPP), as well as driftable halogen anions (Cl⁻) that effectively modulate the energy band diagram and charge carrier transport dynamics of the OCMs, 96 distinct conductance states with linearity approaching 0.98, ultralow power consumption of pW/bit range and symmetric modulation characteristics are demonstrated in the molecular HDD. Combing the associated multi-bit operation and molecular-level spatial resolution potential, data density of the organic storage system can be effectively improved in comparison to traditional magnetic HDDs. More importantly, symmetric switching between consecutive conductance states in the present molecular HDD greatly simplifies the execution of Boolean logic in single storage unit in one step, which is otherwise in-no-way to be realized by asymmetric conductance modulation devices. *In-situ* bitwise encryption of the stored massive data, for instance high-definition replicas of the painted murals in Mogao Grottoes, are showcased through single-unit XOR

manipulation with the SAM based molecular HDD.

RESULTS

Molecular design and fundamental conductance modulation characteristics

Being similar to the magnetic hard-disks, molecular HDD uses mechanical programming heads to write digital information into the physicochemical states of the organic functional molecules, and sense the stored data in terms of tiny bit currents (Fig. 1a). Herein, we deliberately design an organometallic complex Ru^xLPH , consisting of an organic capping ligand carbazolyl terpyridine (CTP), a redox-active ruthenium cation and an anchoring ligand terpyridyl phosphonate (TPP) to assemble the OCMs onto ITO conductive substrates (Fig 1b and Supplementary Fig. 1-8). Note that electron transfer associated with the coordination bonds between Ru cation and CTP/TTP ligands will lead to partial reduction of the former to a lower oxidized state Ru^{x+} with $2 \leq x < 3$. In the meanwhile, the ligands become positively charged as $(\text{CTP}/\text{TPP})^{(3-x)+}$. Under external electric field, counter-balanced redox reaction occurs reversibly between the metal cation and organic ligands,



whereas the existence of chloride anions inside the OCM always maintain the SAM electrically neutral. More critically, the chloride anions undergo local directional drifting as driven by electric field. The resultant build-in potential, arising from the Cl^- accumulation near either surface of the SAM, modifies the net electric field addressing on the OCMs. As an overall effect of the reversible redox reaction and local anion drifting, the conductances of the OCMs will be modulated continuously. As such, multi-bit, low-power programming of digital information can

be achieved through switching the conductance states of OCMs in Ru^XLPH based self-assembly monolayer that serves as storage medium of the molecular HDD.

Fig. 1c and 1d depict the dc current-voltage response and conductance evolution curve of the Ru^XLPH SAM based molecular HDD, which is operated with a conductive-atomic force microscope tip as the programming head to write and read the digital information stored as the molecules' redox and ion accumulation state (Supplementary Fig. 9 and 10). Data writing is executed by applying biased voltage through the programming head onto the OCMs monolayer. As shown in Fig. 1c, the Ru^XLPH OCMs are first scanned in dual-directions, between 0 V to +3.0 V and 0 V to -3.0 V with a ramping step of +0.05 V/-0.05 V. Starting from sampling point #1, the initial conductance of the OCMs is 14.5 nS (Fig. 1d). As the voltage increases, the OCMs conductance drops exponentially to 1.20 nS at 0.1 V and 0.24 nS at 0.5 V (sampling point #2), respectively. Then the I-V curve becomes flat, and the conductance finally reaches 0.06 nS at sampling point #3 with the applied voltage of 3.0 V. Continuous modulation of the OCMs conductance, as expected, may be arising from the oxidization of lower-oxidized state Ru^{x+} ions towards the trivalent form, which in turn modifies the bandgap and conductivity of the organic molecules. Back sweeping to 0 V experiences an immediate steep decreasing of the monitored current, which is accompanied by a polarity reversal of the OCMs' conductance. The conductance is -0.04 nS at sampling #4 of 2.9 V and increases to -0.40 nS at sampling point #5 of 0.5 V. Reversing of the conductance polarity is attributed to the accumulation of Cl⁻ ions attracted by the positively biased programming head near the Ru^XLPH SAM top surface, wherein the establishment of an additional up-pointing build-in potential can offset the external

electric field, therefore influencing the overall effect of the electric field on the charge carrier transport across the organic molecules. At 0 V voltage, the OCM conductance is -36.18 nS. Note that each data point in Fig. 1 and subsequent Fig. 3 represents the average value of 5 individual measurements.

The lineshapes of the I-V and G-V curves recorded during the negative sweeps well resemble that of the positive branch, only minorly differing in the absolute current or conductance values. When swept from 0 V to -3.0 V, the OCMs conductance decreases abruptly from 22.14 nS at 0 V (sampling point #6) to 1.27 nS at -0.1 V and 0.25 nS at -0.5 V (sampling point #7), respectively. Again, the I-V curve becomes flat in the -0.5 V to -3.0 V range, and the conductance reaches -0.06 nS with a polarity reversal at -3.0 V (sampling point #8). Back scanning to 0 V shows a conductance of -0.08 nS at sampling point #9 of -2.9 V and -0.41 nS at sampling point #10 of -0.5 V. Due to the quasi-reversible redox reaction between the metal cation/organic ligands, as well as local drifting of chloride anions, the OCMs' final conductance programmed by C-AFM tip returns to -23.47 nS at 0 V. Note that remarkable conductance windows of $\Delta G = G_{\#2} - G_{\#5} = 640$ pS or $\Delta G' = G_{\#10} - G_{\#7} = 660$ pS are achieved (Fig. 1e), with sampling points #2 and 7 representing the OFF state and sampling points #5 and 10 denoting the ON state. Together with the continuous modulation capability, multi-bit information storage is made possible with the Ru^XLPH samples. Multiplying the monitored current and programming voltage suggests that the peak power consumption is only ~ 690 pW, therefore fulfilling the low-power operation requirements for molecular hard-disks (Fig. 1f). Nevertheless, the spatial resolution of the Ru^XLPH sample is merely limited by the 25 nm

frontend radius of the C-AFM tip. As estimated by an atomic force microscope, the number of Ru^XLPH molecules constituting a basic molecular HDD unit is ~ 235 (Supplementary Fig. 11). It is therefore reasonable to hypothesize that the extremum bit area and operation power can be shrunk by 235 times to $25 \text{ nm}/235 = 1.1 \text{ \AA}$ and $690 \text{ pW}/235 = 2.94 \text{ pW}$, respectively, depending on promising advances achieved in the technical availability of ultra-miniaturized programming heads for massive storage applications.

Conductance modulation mechanism

X-ray photoelectron spectroscopic (XPS) measurements were conducted at room-temperature to confirm the solid-state electrochemistry related conductance modulation mechanism of the Ru^XLPH SAM samples. According to the literature⁴², the Ru 3d_{5/2} binding energies (BEs) of the Ru^XLPH molecules are 280.7 eV for Ru²⁺ and 281.3 eV for Ru³⁺ components, respectively. As plotted in Fig. 2a, both the divalent and trivalent Ru ions appear in the OFF state Ru^XLPH SAM sample. The co-existence of the Ru²⁺ and Ru³⁺ species are in good agreement with the occurrence of ground state electron transfer through the coordination bonds between the Ru³⁺ cation and CTP/TTP ligands pair, which leads to partial reduction of the trivalent cation to a nominal lower oxidized state Ru^{x+} with $2 \leq x < 3$. Integrating along the XPS curve indicates that the Ru²⁺ components share 48.9% of the total metal content, while the Ru³⁺ part occupies 51.1 percent. In addition to the Ru···N coordination bond (18.7%) and amine nitrogen species (-N=, 12.2%) at the binding energies of 398.9 eV and 401.4 eV, respectively, the large amounts of N-C components (69.1%) at the BE of 400.9 eV apparently exceed that of the carbazole groups of the CTP ligand (Fig. 2b). It can be ascribed to the newly appeared positively charged nitrogen atoms, as a result of the oxidization of the pyridine nitrogen through electron transfer to the Ru

cation upon Ru \cdots N coordination. In accordance with the conductance modulation mechanism that the Ru $^{x+}$ cations become effectively oxidized into Ru $^{3+}$ in the ON state, the relative amount of the latter component increases to 73.2% when the Ru XLPH SAM sample has been stressed with a 10 V voltage. Following the reduction of the initially positively charged terpyridine nitrogen atoms, the N-C content decreases to 40.2%, while the Ru \cdots N coordination bonds and -N= species share 30.3% and 20.4%, respectively. Such redox characteristics of the Ru XLPH SAM sample are in good accordance with its electrochemical properties, which have been already reported in our previous work showing reversible cyclic voltammetric transition with the onset oxidization and reduction potentials of 0.84 V and -1.08 V, respectively⁴³.

To better understand the redox-related charge carrier transport properties of the Ru XLPH based SAM samples, the static electronic scenarios of both the divalent and trivalent OCMs are investigated through molecular simulation using the Gaussian program package and the density functional theory (DFT)^{44,45}. As shown in the left panel of Fig. 2c, the Ru ^{II}PLH molecule with divalent ruthenium cation shows continuous positive electrostatic potential (ESP) channel in light red color throughout the entire OCM, with the nitrogen atoms of the terpyridine ligands bearing negative ESP spots (blue) and serving as electron accepting centers in the organometallic complex. Due to the cationic nature of the Ru $^{2+}$ ion, it also displays negative ESP potential in the coordination bond. The energy bandgap associated with the lowest unoccupied molecular orbital (LUMO) and highest occupied molecular orbital (HOMO) energy levels, and the dipole moment of the Ru ^{II}PLH molecule, are 0.626 eV and 10.974 Debye, respectively. Note that electron clouds reside over the entire terpyridine-Ru $^{2+}$ -terpyridine

coordinated chromophores in the HOMO and LUMO orbitals, which is in good agreement with the occurrence of electron transfer between the metal cation and CTP/TTP ligand pairs. When the divalent Ru cation is fully oxidized into the Ru³⁺ form with the terpyridine ligands reduced to the neutral state, obvious reconfiguration of the coordination bonds is visualized (right panel of Fig. 2c). The electrochemical reaction slightly intensifies the HOMO-LUMO energy level difference of the OCM, which increases to 0.635 eV in the Ru^{III}LPH molecule and makes the SAM sample less conductive with relative difficulty of charge carrier transition across the bandgap. Ru^{III}LPH also shows a larger dipole moment of 13.838 Debye, which is favorable for maintaining the as-reached redox and conductance states. As such, modulation of sample conductance exhibits non-volatile nature that is required for long-term data archiving applications. It should also be noted that during molecular simulation the counter anions are fixed to the OCMs through covalent bonds for the ease of calculation convergence. This may lead to minor deviation of the HOMO/LUMO energy levels from the actual values. Nevertheless, the widened bandgap of Ru^{III}LPH will result in device transition into a relatively lower conductance state.

The local drifting of the chloride anions was further assured by the evolution of piezo force microscopic (PFM) phase signals of the self-assembled Ru^XLPH monolayer recorded in different redox states (Fig. 2d). After loading external voltages or electric fields onto the SAM sample through the programming head, the polarization features of the monolayer were characterized *in-situ* in PFM mode. As shown in Supplementary Fig. 9, the as-deposited Ru^XLPH sample has a nanograin morphology inherited from the ITO substrate. Staying in

the pristine state, the mix-valent SAM sample show blue- and yellow-color regions with the respective areal ratios of 47.7% and 52.3%. They correspond to the initial random distribution of chloride anions in the SAM that leads to almost equally aligned up- and downward pointing polarizations. When a voltage of 2.0 V is applied, the color scheme of major area of the Ru^XLPH monolayer turns into white, with minor region becomes blue. It suggests that the net-upward pointing polarization of the molecular HDD basic unit is greatly intensified, which is correlated with the upward drifting of chloride anions under the stimuli of external positive electric field. Their accumulation near the surface of the monolayer results in large amounts of negative charges and greatly enhances the attractive interaction between the programming head and the SAM sample. As the programming voltage projected onto the SAM sample increases to 4.0 V, the total area of the upward pointing polarization region extends to 100% with a maximum PFM signal of 0.012, corresponding to a great extent of chloride ion drifting to the head/SAM interface. Further increase in the amplitude of the programming voltages amplifies the PFM signals continuously. In addition, as the spatial separation between the charged Ru^XLPH framework and counter anions results in the formation of molecular dipoles, changes in dipole moment of the organometallic complex molecule upon transition between various oxidized states (which is visualized through molecular simulation as discussed above), double assure that the relative positions of the chloride ions with respect to the molecular framework are changed⁴⁶⁻⁴⁹. As reported in the literature, local drifting of the counter anion and changes in their relatively position with the molecular framework also influence the width of the molecular energy bandgap⁴⁶. Therefore, the electric field-induced ion drifting, participating in the continuous modulation of the OCMs conductance, is confirmed experimentally in the present

SAM samples.

Based on the above discussion, we try to sketch a phenomenological model that describes the physicochemical process accounting for the multi-bit, low-power conductance modulation of the OCMs in Ru^XLPH based self-assembly monolayer (Fig. 2e). At sampling point #1, the oxidized state of the OCM ruthenium cation is between divalent and trivalent, while the chloride anions are distributed evenly across the entire monolayer. The nitrogen atoms on the CTP/TPP ligands become partially oxidized to compensate the positive charges lost by Ru^{x+} upon electron transfer through the formation of Ru···N coordination bonds (not shown for ease of illustration). When positive voltage of 0.5 V is applied onto the SAM sample, the lower-valent ruthenium cation becomes oxidized toward the trivalent form with the chloride anion drifting toward the monolayer upper surface. At sampling point #3 with sweeping voltage of 3.0 V, 95% of the Cl⁻ anions are accumulated near the SAM surface, resulting in a significant upward pointing build-in potential that modify the net electric field addressing on the Ru^XLPH based monolayer. As the drifting and accumulation of chloride anions continue during back-scanning, the build-in potential completely offsets the influence of the external electric field at the biased voltage of 2.9 V. Afterwards, the polarity of the net electric field across the monolayer reverses, and the OCMs conductance becomes negative. Further scanning with positive voltage continuously increase the absolute value of the negative conductance of the OCMs, resulting in a large memory window when reading at sampling points #5 and #2 with the same stressing voltages of 0.5 V. Sweeping in the negatively biased branch results in similar conductance modulation and polarity reversing behaviors, as shown at sampling points of #6 to #10, which can be

ascribed to the reduction of the Ru^{3+} species to a lower valent form accompanied by the downward drifting of chloride anions towards the $\text{Ru}^{\text{X}}\text{LPH}$ monolayer bottom surface. Note that oxidization of the mixed-valent $\text{Ru}^{\text{x+}}$ to Ru^{3+} cations only occurs in the positive branch to decrease the conductance of the OCMs, while reduction of the trivalent Ru^{3+} to Ru^{2+} cations only takes place in the negative branch to increase the conductance of the OCMs. Therefore, the symmetric conductance modulation characteristics is mainly attributed to the chloride ion drifting induced build-in potential that continuously modifies the net electric field addressed on the $\text{Ru}^{\text{X}}\text{LPH}$ molecules to deliberately control their charge carrier transport dynamics.

High-density data storage performance

A substantial number of conductance states are crucial for enhancing the unit storage density of molecular hard-disks. In order to evaluate its potential for ultrahigh density data storage application, we further assess the current-voltage characteristics of the self-assembled $\text{Ru}^{\text{X}}\text{LPH}$ monolayer in a wider voltage scanning range. As plotted in Fig. 3a, rhombus shape I-V curves with symmetric and continuously expanding hystereses (memory windows) are demonstrated, when the stopping voltage increases from ± 0.5 V to ± 10.0 V with a ramping step of 0.1 V. For instance, the memory window read at the sampling points #2 and #5 with the stressing voltage of 0.5 V (or at the sampling points #7 and #10 with the stressing voltage of -0.5 V) is 222 pS, when the scan stopping voltages are set as ± 0.5 V (Fig. 3b). In case that the scan stopping voltages are 5.5 and 10.0 V, the memory windows are leveraged to 1697 pS and 2907 pS, respectively (Fig. 3c and 3d). Being attributed to the continuous modulations of counter-balanced redox reaction between the $\text{Ru}^{\text{x+}}$ cations and terpyridine ligands, as well as local

drifting and accumulation of the chloride anions, the incremental hystereses are highly favored to increase the number of memory states and thus unit storage density of the Ru^XLPH monolayer based molecular HDD. On the other hand, although the application of ± 10.0 V voltage to the SAM layer with an estimated thickness of ~ 2.54 nm (length of the organometallic complex molecules read by molecular simulation) will generate a high field of 4×10^9 V/m, the possibility that the above discussed conductance modulation characteristics is attributed to electrical breakdown of the organic samples can be safely ruled out. Generally, electrical breakdown is accompanied by thermal pyrolysis related formation of carbon rich conductive filaments in the organic layer. It short-circuits the top and bottom electrodes, which causes large and unswitchable sample currents reaching the compliance level of the measuring instrument. On the contrary, the Ru^XLPH based molecular HDD units demonstrate reprogrammable conductance modulation characteristics with pA level sample currents observed during our measurements, confirming that its origin is intrinsic to the changes of organic molecules' properties.

We also calculate the conductance values of the SAM sample at 0.1 V, as illustrated in Fig. 3a and 3e. Upon increasing the magnitude of the voltage stimuli from 0.5 V to 10.0 V, the OCMs conductance increases from 0.4 to 7.3 nS in the positive sweeps. Reversing the scanning polarity leads to similar conductance modulation characteristics between 0.2 and 8.3 nS. Such symmetric conductance tuning takes place in 96 steps with modulation linearity approaching 0.99 and uniformity exceeding 94% (Supplementary Note 4), therefore enabling at least 6-bit storage for high-density data archiving applications. Accordingly, the disk volume required to

store the same amount of information with the Ru^XLPH monolayer based molecular HDD can be effectively reduced to 16.7% (1/6), in comparison to that of the traditional binary magnetic hard disks. As the 96-state conductance modulation characteristic is demonstrated with the modulating voltages increasing in a ramping step of 0.1 V, further decreasing in the ramping step (e. g. to 0.01 V) may effectively increase the numbers of conductance states in orders of magnitudes approaching that reported in metal oxide based memristor devices⁵⁰. Nevertheless, the 96-state conductance modulation performance is among the best results recorded so far for organic and molecular electronic devices. Moreover, the Ru^XLPH SAM exhibits promising stability and reliability of conductance modulation. 10 out of 96 conductance states, which are obtained with the maximum scanning voltages increasing from 1.0 V to 10.0 V with a ramping step of 1.0 V and read voltage of 0.1 V, are further evaluated for the modulation uniformity and retention capabilities. As plotted in Supplementary Fig. S13, scanning over a single sample for 3 continuous times or scanning over 5 samples reveals that the recorded I-V curves well overlap with each other, showing high cycle-to-cycle and device -to-device uniformities of 98.59% and 96.95% for the OCMs conductance (Fig. 3f and 3g). These conductance states demonstrate good retention performance over 10000 s (Fig. 3h). Although a maximum fluctuation of 15.20% is observed during operation, these 10 conductance states under evaluation are still distinguishable from each other and thus suggest their applicability for data storage usage. Herein, the conductances were read by applying a triangle voltage signal with peak value of 0.1 V and width of 966 ms on the atomic force microscope, wherein the continuous stressing with electrical stimuli may change the sample conductances non-negligibly. In case a short pulse instead of triangle wave is used, a smoother retention curve can be expected reasonably. The

conductance modulation performance can be maintained under low temperatures approaching that of the liquid nitrogen (Supplementary Fig. 14), again assuring the stability of the present molecular HDD in various working environments. As mobile ions are frozen at low temperatures, the build-in potential arising from ion migration and accumulation, as well as the net electric field addressed on the SAM layer, can be modified significantly in comparison to that established at room temperature. The degree of sample conductance modulation is attenuated consequently, giving rise to obviously shrunk hystereses in the I-V curves shown in Supplementary Fig. 14.

Implementation of Boolean and high-order molecular logics

Encryption *via* bit-wise logic manipulation on the stored information can enhance the security level of massive confidential data. In addition to the feasibility of utilizing conductance modulation to execute logic operators⁵¹⁻⁵⁵, its nonvolatile characteristic also allows *in-situ* storage of the computing outputs, which eliminates the necessity of involving additional storage spaces or operations to stock the genuine and newly generated data. As the most general candidates, Boolean logics have been widely demonstrated through on-demand manipulation of conductance in memristive devices⁵⁶⁻⁵⁸. Upon one- or two-step input of voltage-based modulating signals, pairing between the initial and final conductance states of a single molecular HDD unit can simply deliver 14 out of 16 Boolean logic operations (Supplementary Fig. 15 and Supplementary Table 1). The remaining XOR operator requires two HDD units to be implemented, while the XNOR gate cannot be achieved technically with the Ru^XLPH molecular HDD (Fig. 4a, 4b and Supplementary Fig. 16). XOR gate is of great importance for information security applications⁵⁹⁻⁶¹. As its two-unit operation methodology based on bistable

conductance modulation characteristic of molecular HDD is unable to achieve bit-by-bit encryption of the stored data, more efficient approach should be developed to securely encode the confidential information.

Remembering that beyond the bistable conductance modulation behavior, Ru^XLPH molecules also exhibit bidirectionally symmetric switching characteristics. With such unique feature, we are able to design a single-HDD-unit based one-step algorithm to impart XOR logic operation. As shown in Fig. 4c, programming voltage stimuli of 0 V or 2.5 V are applied through the C-AFM tip and ITO electrode simultaneously as V_p and V_q . The difference V_{p-q} , which is the actual voltage applied to tune the OCMs conductance, is defined as the logic input. Before operation, the Ru^XLPH molecules reside in the logic “0” state with initial high conductance of 14.5 nS. Then, voltage stimuli of V_p and V_q are applied to control the OCMs status. When V_p and V_q equal each other, V_{p-q} and input signal are “0”. The OCMs conductance remains unchanged to deliver a logic output of “0”. When V_p and V_q are different, V_{p-q} is ± 2.5 V and input signal is defined as “1”. In case that V_{p-q} is +2.5 V, the low-valent Ru^{x+} species are oxidized into trivalent Ru³⁺ ions. In the meanwhile, the chloride anions drift towards the positively biased programming tip, resulting in an upward pointing build-in potential in the molecular monolayer. As such, the OCMs conductance is reduced to 63.8 pS and output logic state “1”. If the V_{p-q} is -2.5 V (in the backward scan), the trivalent Ru³⁺ cations are reduced to the divalent Ru²⁺ form, with the chloride anions accumulated near the SAM/ITO surface to give a downward pointing build-in potential. The OCMs conductance is 92.8 pS and logic output signal is also “1”. Fig. 4d and 4e summarize the truth table and simulated results of the single-

HDD-unit based XOR operation schemes. In comparison to other conductance modulation related device approaches, the symmetric-switching molecular HDD logic outperforms obviously in terms of unit numbers and operation steps (Supplementary Table 2), not only favoring the reduction of storage space and computing costs but also enabling bit-level encryption of the stored data.

The continuous conductance modulation of the Ru^XLPH based molecular HDD also allows the design of high-order logics, which may further simplify the spatial and temporal complexity of computing algorithm⁶²⁻⁶⁴. For demonstration, we show a computationally complete set of the ternary logic that is closest to the binary counterparts and can be implemented in a single molecular HDD unit, including operators of Plus MAX, Multiply MIN, and Threshold Comparison according to our previous work^{65,66}:

$$f(x) = \max(p,q) \quad (2)$$

$$f(x) = \min(p,q) \quad (3)$$

$$f_k(x) = \begin{cases} 2, & x = k \\ 0, & x \neq k \end{cases} \quad (4)$$

where p and q are logic inputs while k corresponds to logic states of “0”, “1”, or “2” (Supplementary Fig. 17 and Supplementary Table 3). Theoretically, all ternary operations can be realized by synthesizing the above complete set *via* logic cascading, which also permits downward compatibility with conventional binary Boolean logics. Beyond the ternary participators, even higher-order operators of quaternary logics can also be demonstrated with a single molecular HDD unit, as shown in Supplementary Fig. 18 and Supplementary Table 4.

***In-situ* encryption of stored Mogao Grottoes Mural picture.**

Finally, we demonstrate the possibility of using molecular HDD as a logic operator protocol for encrypted massive data storage, using the digital image of Mogao Grottoes Mural as an example. A part of the chromatic Bodhisattva mural in Cave 205 is compressed into a 128×128 (16k pixel) image and further decomposed into three monochromatic pictures of the red (R), green (G) and blue(B) primary colors (Supplementary Fig. 19 and Fig. 5a). To make full use of the 96-memory states of the Ru^XLPH molecules, the grey-scale values of the monochromatic pixels are divided into 64 levels. Each pixel in these monochromatic images, therefore, can be vividly represented by a 6-bit binary digit. Using traditional binary magnetic HDDs, 18 (6×3) units are required to store the image information of a single pixel, and the entire chromatic mural image consumes $128 \times 128 \times 18 = 294912$ units. Due to the multi-bit memory capacity of the Ru^XLPH molecules, each pixel of the molecular HDD only utilizes three units to represent the RGB information. As such, the mural image costs far less of $128 \times 128 \times 3 = 49152$ units to fully store the genuine visual information. In other words, the Ru^XLPH based molecular HDD is particularly effective for massive data storage. Supplementary Table 5 and Supplementary Fig. 20 summarize the encoding table and 6-bit pixel greyscale values matrices of the RGB decomposed mural image.

As sketched in the encryption data flowchart of Fig. 5b, the binary pixel intensity information and its monochromatic greyscale value sub-matrices of the mural image are defined as plaintexts. Three sets of encryption key matrices, corresponding to the RGB domains and containing 128×128 numeric strings of 6-bit binary digits each, are generally randomly through the Python function of randint. For each pixel of the monochromatic sub-matrices, bit-by-bit

XOR operation between its plaintext of the 6-bit greyscale value and random key results in a ciphertext of new numeric string. Note that the XOR operation outputs “0” when the binary digits of the input pairs are the same. On the contrary, the operator outputs “1” when the input pairs are different. Reading from Supplementary Files 1-3 and Supplementary Fig. 20-22, the 6-bit greyscale value plaintext, encryption key and ciphertext groups are (110101, 010110, 100011), (000100, 110010, 110110) and (001000, 010000, 011000) for the first pixel of the mural image in the RGB domains, respectively. These encryption operations are simulated by applying voltage stimuli with intensities of 4.0 V (back scan), 5.5 V and 2.9 V to the Ru^XLPH based molecular HDD unit to program its conductances to new levels, which are then read and decoded similarly to deliver the ciphertexts (Fig. 5c). Encrypting along the 128×128 monochromatic sub-matrices, following by superimposing the resultant ciphertexts, the mural image can be completely translated into an unreadable mosaic pattern to enhance the data security level (Fig. 5d). The second-round execution of XOR operations between the ciphertext and encryption key matrices then leads to symmetric decryption of the encrypted data. Beneficial from the non-volatile nature of OCMs conductance modulation, both plaintexts and ciphertexts of the mural image can be stored *in-situ* in the same molecular HDD units, greatly conserving the hardware consumption for encrypted massive data storage. Again, it should be emphasized that without the possibility of executing single-unit XOR operation through symmetric conductance modulation, the critical *in-situ* bitwise encryption of the stored data is unable to be realized for the next generation information techniques.

DISCUSSIONS

In summary, we designed an organometallic complex molecule Ru^XLPH consisting of a mixed-valent Ru^{x+} cation and terpyridine based organic ligand pairs. Due to the occurrence of counter-balanced redox reaction between metal cation and ligands, as well as local drifting of chloride anions, the Ru^XLPH SAM based molecular HDD exhibits bidirectional, symmetric and continuous conductance modulation with large memory windows. It not only benefits the realization of high-density data storage through multi-bit operation, but allows implementation of *in-situ* bitwise encryption of the stored information, which is highly desired for the storage of massive confidential data in modern society. In addition, control experiments and simulations were conducted to make a double assurance that the observed conductance modulation characteristics are arising from the inherent properties of the organometallic complex molecules. As shown in Supplementary Fig. 23, replacing the transition metal cation Ru^{x+} with Os^{x+} results in rhombus shaped current-voltage curves with similar conductance modulation characteristic, which is accompanied by the variation of molecular energy bandgaps in different oxidized states. As the absolute conductance values of the Os^XLPH molecules are thirty times smaller than that of the Ru^XLPH molecules, it can be concluded confidentially that the conductance modulation behaviors observed in the molecular HDD are material-specific. The incorporation of other counter anions such as fluoride (F⁻) and hexafluorophosphate (PF₆⁻) also influence the changes of molecular orbitals upon transition between different oxidized states (Supplementary Fig. 24), as well as conductance modulation characteristics⁴⁶. Note that since the environmental moisture significantly affects the electrical performance of the Ru^XLPH SAM samples (Supplementary Fig. 25), proper encapsulation of the molecular HDD should be carried out for practical applications. In the future, combining the deliberate

molecular design cum synthesis strategy, partitioned assembling of customized molecules, and use of flexible substrates, the molecular HDD may even evolve into floppy disks for high-density, high-security portable digital gadgets.

METHODS

Synthesis and characterization. Synthesis details of the organic and organometallic complex molecules are provided in Supplementary Section 1 and Supplementary Fig. 1-8. The ^1H , ^{13}C , and ^{31}P nuclear magnetic resonance (NMR) spectra were recorded using a Bruker AV-500 spectrometer at 25 °C. Matrix-assisted laser desorption/ionization-time-of-flight (MALDI-TOF) and electrospray ionization (ESI) mass spectrometry (MS) were performed using a Bruker Daltonics Autoflex III TOF.

Electrical measurement. A nanoscale test structure of Pt/Ru^XLPH SAM/ITO was constructed as the basic storage and logic unit of molecular HDD for electrical measurement. The platinum tip of a conductive-atomic force microscope (C-AFM, FastScan Bio) was used as the programming head of the molecular HDD while the ITO substrate served as a universal bottom electrode. All electrical measurements were conducted on the AFM in ambient environment with a relative humidity of ~33% (except for otherwise mentioned). A linear amplifier with single-channel measurement capability and spatial scanning rate of 1.3 Hz is used for the current-voltage measurements in DC voltage sweeping mode. Sample conductance was calculated as the quotient of as-recorded C-AFM current signal divided by programming or reading voltages. The electrical characteristics of the Os^XLPH SAM samples were measured similarly.

Molecular Simulation. All density functional theory (DFT) calculations were performed using Gaussian 09 package^{44,45}. For better comparison between different charged molecules, all states for geometry optimization are in singlet and close shell. The B3LYP functional was used for geometry optimization. The 6-31G(d) basis set was used for the C, H, O, N and P atoms, while LANL2DZ and its corresponding pseudopotential was used for Ru and Os atoms. All geometry optimization was done in the gas phase.

Logic and encrypted data storage demonstration. The logic and *in-situ* encrypted data storage operations were investigated using Cadence Virtuoso platform. During simulation, the conductance modulation characteristics of the SAM samples were used as experimental inputs.

DATA AVAILABILITY

The authors declare that all data supporting the findings of this work are included in the article and Supplementary Information files.

AUTHOR CONTRIBUTIONS

M. L and G. L conceived the idea. J. W. synthesized and characterized the molecules. B. G., W. X. and P. W. conducted the electrical measurements. A. C. and J. L. performed the molecular simulation. X. C, B. G., Z. W., X. Z. and J. Z. carried out the logic and data encryption simulation. B. G., X. C., A. C. analyzed and visualized the experimental data. B. G., X. C., M. L., X. X., Y. C. and G. L. co-wrote the paper. All the authors discussed the results and commented on the manuscript.

CONFLICTS OF INTEREST

There are no conflicts to declare.

ACKNOWLEDGEMENTS

This work is supported by the National Key R&D Program of China (2022YFB4700102). The authors would like to thank Prof. R. S. Stanley and Prof. C. A. Nijhuis for fruitful discussions.

REFERENCES

1. Ling, Q.-D. et al. Polymer electronic memories: Materials, devices and mechanisms. *Prog. Polym. Sci.* **33**, 917-978 (2008).
2. Heremans, P. et al. Polymer and Organic Nonvolatile Memories. *Chem. Mater.* **23**, 341-358 (2010).
3. Chen, Y. et al. Polymer memristor for information storage and neuromorphic applications. *Mater. Horiz.* **1**, 489-506 (2014).
4. van der Burgt, Y. et al. Organic electronics for neuromorphic computing. *Nat. Electron.* **1**, 386-397 (2018).
5. Jiang, J. et al. Organic functional molecules towards information processing and high-density information storage. *Adv. Mater.* **20**, 2888-2898 (2008).
6. Jia, C. et al. Interface-engineered bistable rotaxane-graphene hybrids with logic capabilities. *Adv. Mater.* **25**, 6752-6759 (2013).
7. Zhang, B. et al. Redox gated polymer memristive processing memory unit. *Nat. Commun.* **10**, 736 (2019).
8. Moller, S. et al. A polymer/semiconductor write-once read-many-times memory. *Nature* **426**, 166-169 (2003).
9. Oyamada, T. et al. Switching effect in Cu:TCNQ charge transfer-complex thin films by vacuum codeposition. *Appl. Phys. Lett.* **83**, 1252-1254 (2003).
10. Ouyang, J. et al. Programmable polymer thin film and non-volatile memory device. *Nat Mater.* **3**, 918-922 (2004).
11. Harada, K. et al. Organic homojunction diodes with a high built-in potential: interpretation of the current-voltage characteristics by a generalized Einstein relation. *Phys. Rev. Lett.* **94** 036601 (2005).
12. Colle, M. et al. Switching and filamentary conduction in non-volatile organic memories. *Org. Electron.* **7**, 305-312 (2006).
13. Lim, S. L. et al. Conformation-induced electrical bistability in non-conjugated polymers with pendant carbazole moieties. *Chem. Mater.* **19**, 5148-5157 (2007).
14. Ling, Q.-D. et al. Synthesis and dynamic random access memory behavior of a functional polyimide. *J. Am. Chem. Soc.* **128**, 8732-8733 (2006).
15. Kuorosawa, T. et al. High performance volatile polymeric memory devices based on novel triphenylamine-based polyimides containing mono- or dual-mediated phenoxy linkages. *Macromolecules* **43**, 1236-1244 (2010).
16. Bandyopadhyay, A. & Pal, A. J. Tuning of organic reversible switching *via* self-assembled supramolecular structures. *Adv. Mater.* **15**, 1949-1952 (2003).
17. Sivaramakrishnan, S. et al. Controlled insulator-to-metal transformation in printable polymer composites with nanometal clusters. *Nat. Mater.* **6**, 149-155 (2007).

18. Ma, Y. et al. Metal complex modified azo polymers for multilevel organic memories. *Nanoscale* **7**, 7659-7664 (2015).
19. Bandyopadhyay, A. & Pal, A. J. Multilevel conductivity and conductance switching in supramolecular structures of an organic molecule. *Appl. Phys. Lett.* **84**, 999-1001 (2004).
20. Lauters, M. et al. Multilevel conductance switching in polymer films. *Appl. Phys. Lett.* **89**, 013507 (2006).
21. Zhang, B. et al. 90% yield production of polymer nano-memristor for in-memory computing. *Nat. Commun.* **12**, 1984 (2021).
22. Song, Y. et al. Two memristors-based XOR logic demonstrated with encryption/decryption. *IEEE Electron. Dev. Lett.* **42**, 1398–1401 (2021).
23. Yang, L. et al. Cryptographic key generation and *in situ* encryption in one–transistor–one–resistor memristors for hardware security. *Adv. Electron. Mater.* **7**, 2001182 (2021).
24. Liu, R. et al. Stable Universal 1- and 2-put Single-Molecule Gates. *Adv. Mater.* **34**, 2202135 (2022).
25. Kim, K. M. & Williams, R. S. A family of stateful gates for complete cascading logic. *IEEE Trans. Circuit & Syst.-I* **66**, 4348-4355 (2019).
26. Tseng, R. J. et al. Digital memory device based on tobacco mosaic virus conjugated with nanoparticles. *Nat. Nanotechnol.* **1**, 72-77 (2006).
27. Kim, T.-W. et al. A direct metal transfer method for cross-bar type polymer non-volatile memory applications. *Nanotechnology* **19**, 405201 (2008).
28. de Leeuw, D. W. et al. Crossbar memory array of organic bistable rectifying diodes for nonvolatile data storage. *Appl. Phys. Lett.* **97**, 193308 (2010).
29. Huang, R. et al. Resistive switching in organic memory device based on parylene-C with highly compatible process for high-density and low-cost memory applications. *IEEE Trans. Electron. Dev.* **59**, 3578-3582 (2012).
30. Yoo, D. et al. Vertically stacked microscale organic nonvolatile memory devices toward three-dimensional high integration. *Org. Electron.* **21**, 198-202 (2015).
31. Yin, Y. et al. Direct photopolymerization and lithography of multilayer conjugated polymer nanofilms for high performance memristors. *J. Mater. Chem. C* **6**, 11162-11169 (2018).
32. Ren, Y. et al. Iridium-based polymer for memristive devices with integrated logic and arithmetic applications. *J. Mater. Chem. C* **8**, 16845-16857 (2020).
33. Cuevas, J. C. & Scheer, E. The birth of molecular electronics. *In: Molecular Electronics: An Introduction to Theory and Experiment.* 3-18 (World Scientific, Singapore 2017)
34. Reed, M. A. et al. Conductance of a molecular junction. *Science* **278**, 252-254 (1997).
35. Chen, J. et al. Large on-off ratios and negative differential resistance in a molecular electronic device. *Science*, **286**, 1550-1552 (1999).
36. Collier, C. et al. Electronically configurable molecular-based logic gates. *Science* **285**, 391–394 (1999).

37. Venkataraman, L. et al. Dependence of single-molecule junction conductance on molecular conformation. *Nature* **442**, 904-907 (2006).
38. Williams, R. S. et al. Potential and challenges of computing with molecular materials. *Nat. Mater.* **23**, 1475-1485 (2024).
39. Sharma, D. et al. Linear symmetric self-selecting 14-bit molecular memristor. *Nature* **633**, 560-566 (2024).
40. Li, J. et al. Room-temperature logic-in-memory operations in single-metallofullerene devices. *Nat. Mater.* **21**, 917-923 (2022).
41. Xiang, D. et al. Molecular-scale electronics: From concept to function. *Chem. Rev.* **116**, 4318-4440 (2016).
42. Dey, S. K. et al. Growth and nanostructure of conformal ruthenium films by liquid-source metalorganic chemical vapor deposition. *Appl. Phys. Lett.* **94**, 774-777 (2003).
43. Zhang, J. et al. Rapidly sequence-controlled electrosynthesis of organometallic polymers. *Nat. Commun.* **11**, 2530 (2020).
44. Frisch, M. J. et al. *GAUSSIAN 09*, Revision A.02, Gaussian, Inc., Wallingford, CT, (2009).
45. Zhang, G. & Musgrave, C. B. Comparison of DFT methods for molecular orbital eigenvalue calculations. *J. Phys. Chem. A.* **111**, 1554-1561 (2007).
46. Goswami, S. et al. Robust resistive memory devices using solution-processable metal-coordinated azo aromatics. *Nat. Mater.* **16**, 1216-1225 (2017).
47. Goswami, S. et al. Charge disproportionate molecular redox for discrete memristive and memcapacitive switching. *Nat. Nanotechnol.* **15**, 380-399 (2020).
48. Han, Y. et al. Electric-field-driven dual-functional molecular switches in tunnel junctions. *Nat. Mater.* **19**, 843-848 (2020).
49. Wang, Y. et al. Dynamic molecular switches with hysteretic negative differential conductance emulating synaptic behavior. *Nat. Mater.* **21**, 1403-1411 (2022).
50. Rao, M. et al. Thousands of conductance levels in memristors integrated on CMOS. *Nature* **615**, 823-829 (2023).
51. Terabe, K. et al. Quantized conductance atomic switch. *Nature* **433**, 47-50 (2005).
52. Borghetti, J. et al. 'Memristive' switches enable 'stateful' logic operations via material implication. *Nature* **464**, 873-876 (2010).
53. Yang, J. J. et al. Memristive devices for computing. *Nature Nanotechnol.* **8**, 13-24 (2013).
54. Wong, H. S. & Salahuddin, S. Memory leads to better computing. *Nat. Nanotechnol.* **10**, 191-194 (2015).
55. Goswami, S. et al. Decision trees within a molecular memristor. *Nature* **597**, 51-56 (2021).
56. Wald, N. & Kvatinsky, S. Design methodology for stateful memristive logic gates. *Proc. IEEE ICSEE*. p 1 (2016).
57. Vourkas, I. & Sirakoulis, G. C. Emerging memristor-based logic circuit design approaches: A review. *IEEE Circuits Syst. Mag.* **16**, 15-30 (2016).

58. Gupta, T. et al. Redox-active monolayers as a versatile platform for integrating boolean logic gates. *Angew. Chem. Int. Ed.* **47**, 5322-5326 (2008).
59. Liu, Y. et al. An electrochemically transduced XOR logic gate at the molecular level. *Angew. Chem. Int. Ed.* **49**, 2595-2598 (2010).
60. Song, Y. et al. Two memristors-based XOR logic demonstrated with encryption/decryption. *IEEE Electron. Dev. Lett.* **42**, 1398–1401 (2021).
61. Yang, L. et al. Cryptographic key generation and *in situ* encryption in one-transistor-one-resistor memristors for hardware security. *Adv. Electron. Mater.* **7**, 2001182 (2021).
62. Post, E. L. Introduction to a general theory of elementary propositions. *Am. J. Math.* **43**, 163-185 (1921).
63. Rohleder, H. Three-valued Boolean algebra and its application in the description of switching circuits consisting of bistable contact elements. *Z. AMM* **34**, 308-311 (1954).
64. Goto, M. et al. Theory and structure of the automatic relay computer E. T. L. Mark II. *J. Symbolic Logic* **23**, 60 (1958).
65. Xue, W. et al. Controllable and stable quantized conductance states in a Pt/HfO_x/ITO memristor. *Adv. Electron. Mater.* 1901055 (2015).
66. Zhang, Y.-J. et al. Implementation of all 27 possible univariate ternary logics with a single ZnO memristor. *IEEE Trans. Electron. Dev.* **66**, 4710-4715 (2019).

CAPTIONS FOR FIGURES

Figure 1 Design strategy and basic electrical characteristics of Ru^XLPH SAM based molecular HDD. (a) Schematic illustration of the traditional magnetic and conceptual molecular hard-disk. (b) Design strategy of organometallic complex molecule Ru^XLPH that may exhibit continuous conductance modulation behaviors. (c) DC current-voltage characteristics, (d) conductance evolution curves, (e) distribution of the ON- and OFF-state conductances and (f) conductance-modulation power characteristics of the Ru^XLPH self-assembled monolayer.

Figure 2 Conductance modulation mechanism of Ru^XLPH SAM. (a) Ru 3d_{5/2} and (b) N 1s XPS spectra of the Ru^XLPH SAM in OFF and ON states. (c) HOMO, LUMO and ESP distribution of the Ru^XLPH molecule with Ru²⁺ and Ru³⁺ cations. The brown, white, blue, green, red and light purple spheres represent carbon, hydrogen, nitrogen, oxygen, phosphor and ruthenium atoms, respectively. (d) Evolution of the PFM phase signals of the Ru^XLPH SAM upon being subject to bias voltage of 0 V, 1.0 V, 2.0 V and 3.0 V. (e) A phenomenological model describing the evolution of redox states of the Ru cation as well as the local drifting and accumulation of chloride anions in the Ru^XLPH SAM during biased voltage sweepings.

Figure 3 Multi-level memory performance of Ru^XLPH SAM based molecular HDD. (a-d) DC current-voltage characteristics of the Ru^XLPH self-assembled monolayer, recorded with various maximum scanning voltages of ±0.5 V to ±10.0V. (e) 96-state linear modulation of OCMs conductance during the forward and backward scans, recorded with the maximum biased scanning voltages of 0.5 V to 10.0 V, respectively. (f) Cycle-to-cycle uniformity, (g) device-to-device uniformity and (h) retention characteristics of the OCMs conductances.

Figure 4 Implementations of XOR logic with Ru^XLPH SAM based molecular HDD. (a) Schematic of a XOR logic gate, as well as its implementation with (b) two devices showing traditional redox-related bistable conductance modulation behavior and (c) a single Ru^XLPH based molecular HDD unit exhibiting redox and ion drifting induced symmetric conductance switching characteristic. (d) Truth table and (e) simulated results of the as-designed XOR logic operator.

Figure 5 *In-situ* encryption of a Mogao Grottoes Mural image stored in Ru^XLPH SAM based molecular HDD. (a) Compress and RGB channel generation of a chromatic Bodhisattva mural image in Cave 205 of the Mogao Grottoes. (b) Flowchart of image encryption and decryption through bit-by-bit XOR operations. (c) Simulated data for storing, encrypting and decrypting of the 6-bit greyscale value information of the mural image's first pixel in the RGB channels. (d) Conversion between the genuine chromatic mural image and the encrypted monochromatic and chromatic images.

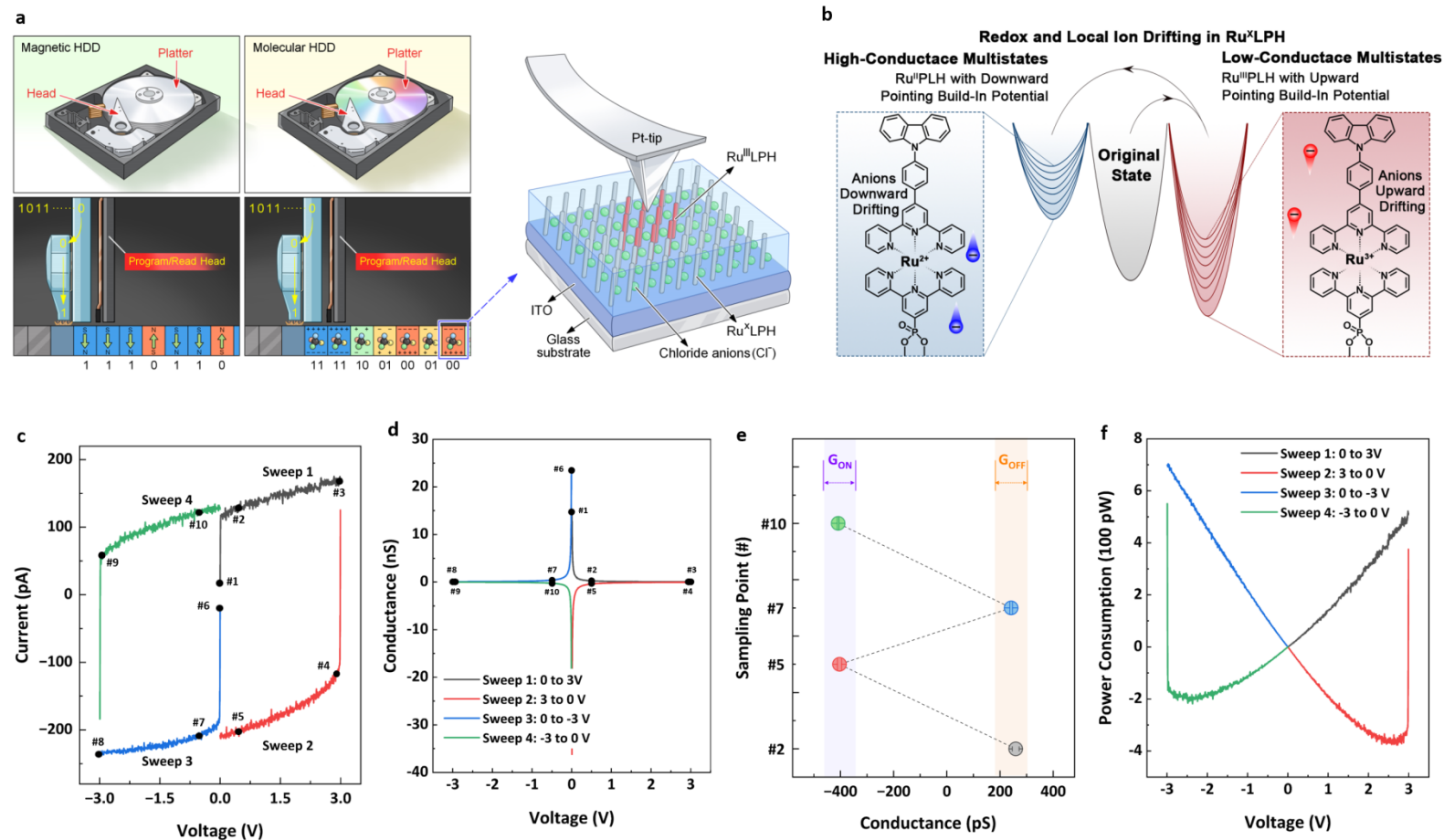


Figure 1 Design strategy and basic electrical characteristics of Ru^xLPH SAM based molecular HDD. (a) Schematic illustration of the traditional magnetic and conceptual molecular hard-disk. (b) Design strategy of organometallic complex molecule Ru^xLPH that may exhibit continuous conductance modulation behaviors. (c) DC current-voltage characteristics, (d) conductance evolution curves, (d) distribution of the ON- and OFF-state conductances and (d) conductance-modulation power characteristics of the Ru^xLPH self-assembled monolayer.

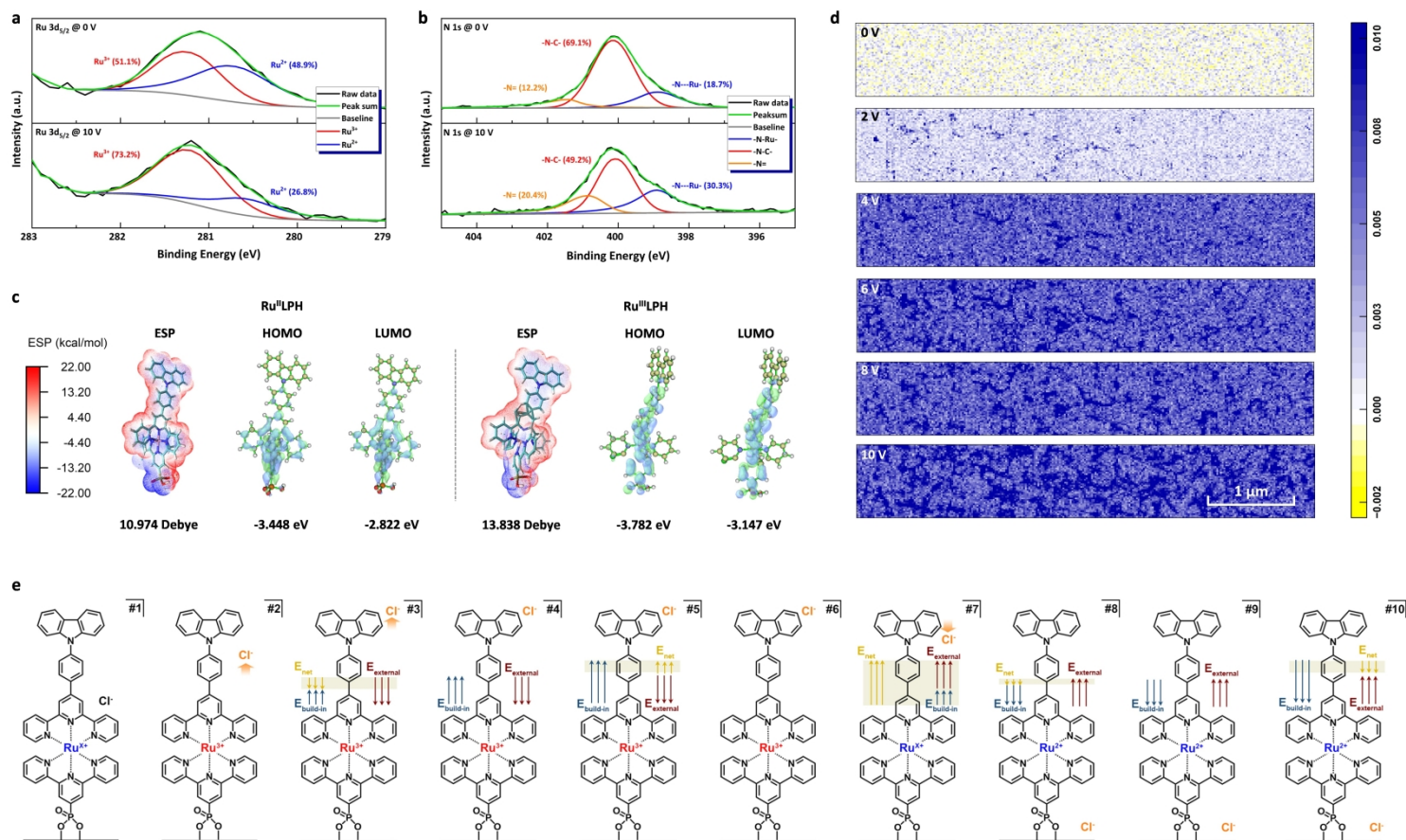


Figure 2 Conductance modulation mechanism of Ru^XLPH SAM. (a) Ru 3d_{5/2} and (b) N 1s XPS spectra of the Ru^XLPH SAM in OFF and ON states. (c) HOMO, LUMO and ESP distribution of the Ru^XLPH molecule with Ru²⁺ and Ru³⁺ cations. The brown, white, blue, green, red and light purple spheres represent carbon, hydrogen, nitrogen, oxygen, phosphor and ruthenium atoms, respectively. (d) Evolution of the PFM phase signals of the Ru^XLPH SAM upon being subject to bias voltage of 0 V, 1.0 V, 2.0 V and 3.0 V. (e) A phenomenological model describing the evolution of redox states of the Ru cation as well as the local drifting and accumulation of chloride anions in the Ru^XLPH SAM during biased voltage sweepings.

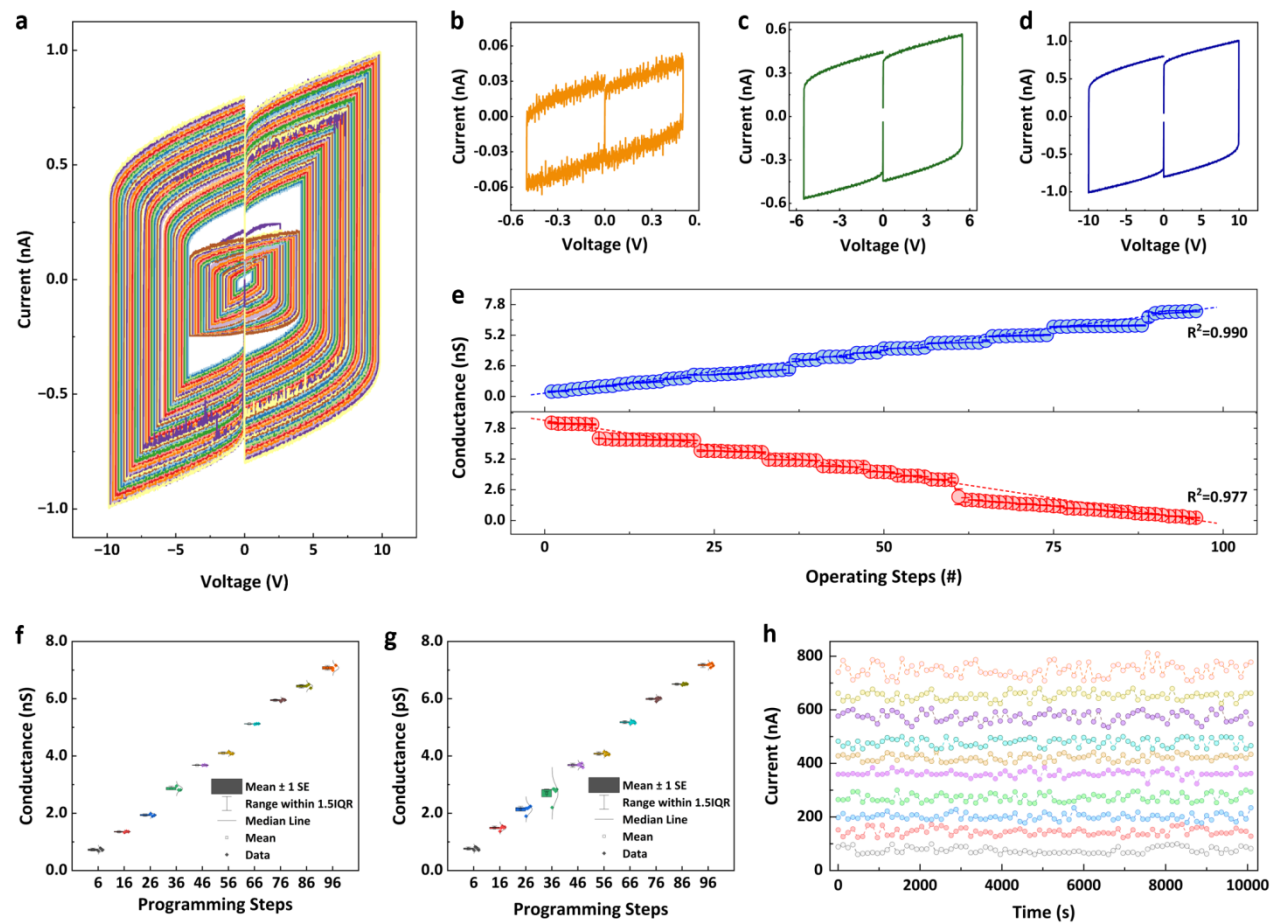


Figure 3 Multi-level memory performance of Ru^xLPH SAM based molecular HDD. (a-d) DC current-voltage characteristics of the Ru^xLPH self-assembled monolayer, recorded with various maximum scanning voltages of ± 0.5 V to ± 10.0 V. (e) 96-state linear modulation of OCMs conductance during the forward and backward scans, recorded with the maximum biased scanning voltages of 0.5 V to 10.0 V, respectively. (f) Cycle-to-cycle uniformity, (g) device-to-device uniformity and (h) retention characteristics of the OCMs conductances.

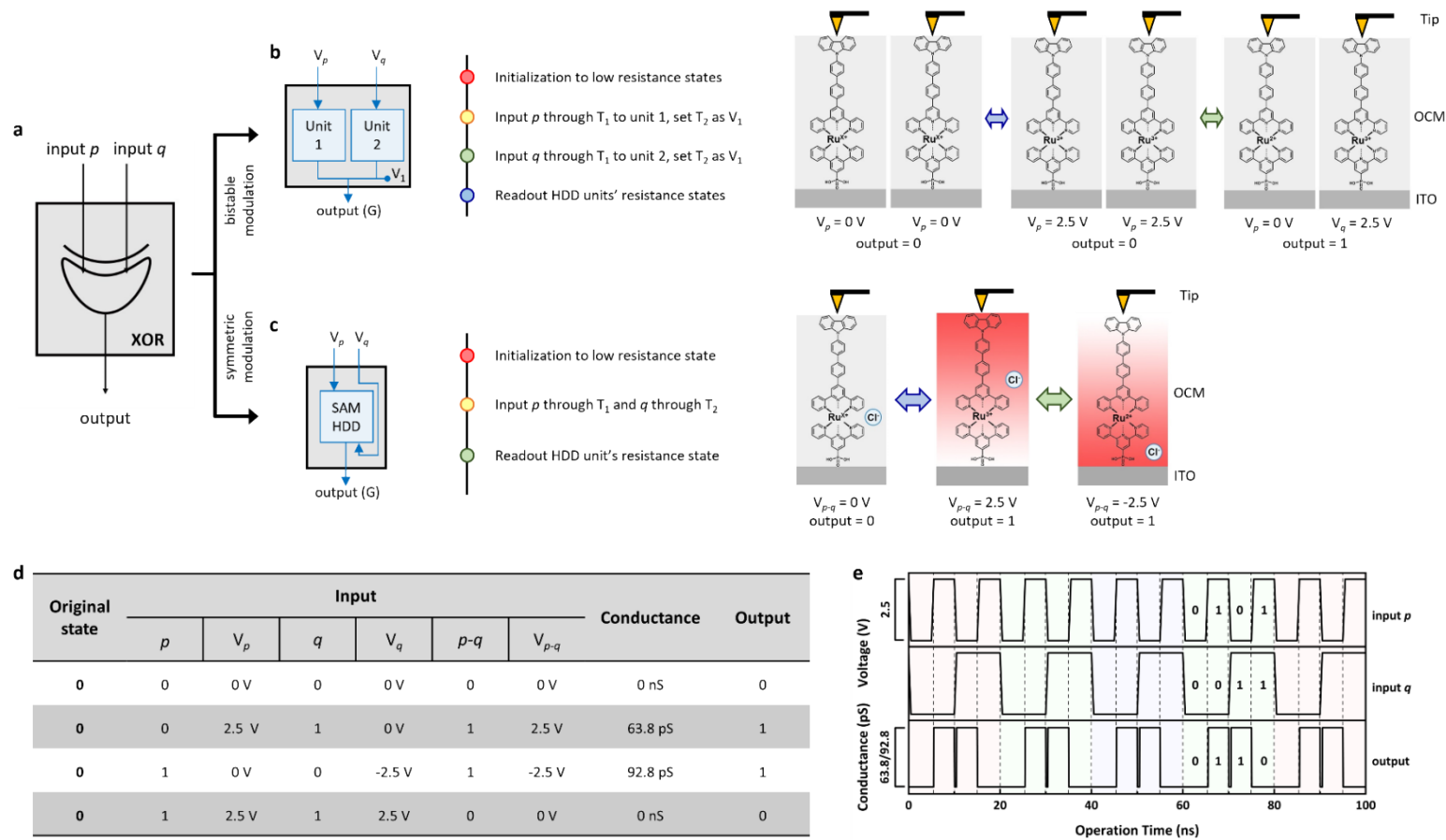


Figure 4 Implementations of XOR logic with Ru^XLPH SAM based molecular HDD. (a) Schematic of a XOR logic gate, as well as its implementation with (b) two devices showing traditional redox-related bistable conductance modulation behavior and (c) a single Ru^XLPH based molecular HDD unit exhibiting redox and ion drifting induced symmetric conductance switching characteristic. (d) Truth table and (e) simulated results of the as-designed XOR logic operator.

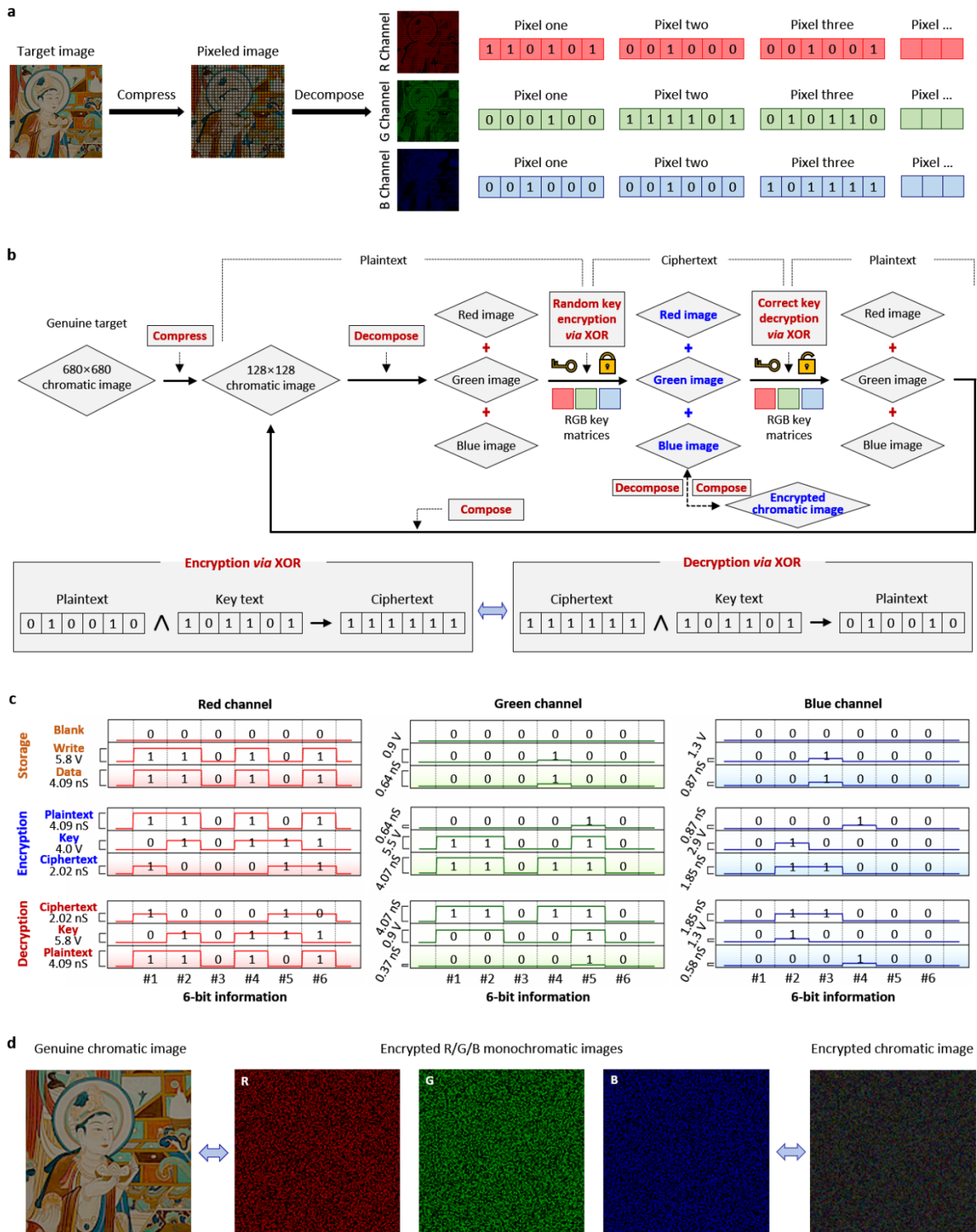


Figure 5 *In-situ* encryption of a Mogao Grottoes Mural image stored in Ru^XLPH SAM based molecular HDD. (a) Compress and RGB channel generation of a chromatic Bodhisattva mural image in Cave 205 of the Mogao Grottoes. (b) Flowchart of image encryption and decryption through bit-by-bit XOR operations. (c) Simulated data for storing, encrypting and decrypting of the 6-bit greyscale value information of the mural image's first pixel in the RGB channels. (d) Conversion between the genuine chromatic mural image and the encrypted monochromatic and chromatic images.